Interpolyelectrolyte Complex and Coacervate Formation of Poly(glutamic acid) with a Dendrimer Studied by Light Scattering and SAXS†

Dietrich Leisner and Toyoko Imae*

Research Center for Materials Science, Nagoya University, Chikusa, Nagoya 464-8602, Japan

Received: October 31, 2002; In Final Form: April 8, 2003

Interpolyelectrolyte complex (IPEC) formation between sodium poly(L-glutamate) and poly(amido amine) dendrimer in aqueous solution containing 0.25 M NaCl was studied as a function of pH by light scattering. The formation of soluble IPECs upon protonation of the dendrimer at 11 > pH > 9.1 was followed from the increase of the extrapolated scattering intensity at zero scattering angle, the indirect Fourier transform method being used for the fitting of the scattering curves and for evaluation of the particle size. Coacervation was observed at pH ∼9.1 which increased slightly with the dendrimer excess. Dynamic light scattering revealed three relaxation modes. The relaxation times τ of the two faster modes scale with the scattering vector q as $\tau \propto q^{-2}$ and are attributed to the diffusion of dendrimer and of microgel inhomogeneity. An additional slow mode ($\tau \propto q^{0}$) dominates the multiexponential dynamic structure factor of the IPEC solutions until breaking down at the pre-transition to the coacervation, which is also associated with a sharp increase of the radius of gyration R_g of mesoscopic particles from ∼50 to ∼250 nm. The microscopic structure of the coacervate was analyzed by small-angle X-ray scattering. The R_g ∼1.7 nm obtained from Guinier analysis of the smooth intermediate scattering function was close to that of a dendrimer. A low-q upturn of the scattering curves $I(q)$ with $I \propto q^{-6}$ was attributed to the superimposed scattering from compact spheres with a radius of ∼20 nm. A high-q upturn exhibits a power-low decay of $I(q) \propto q^{-3}$, which may be attributed to a smooth surface.

1. Introduction

Polyion−polyelectrolyte complexes (PECs) have several applications in separation processes (flocculation), including protein separation,[1,2] colloid stabilization,[3,4] drug delivery systems,[5,6] and thin film[7−9] and membrane preparation.[10−12] Since PEC formation is mainly governed by electrostatics, key parameters are the charge density, geometry (shape and flexibility of the charge distribution), swelling, counterion hydrophilicity, and screening. A spherelike polyion or guest polyelectrolyte (GPE) binds to a linear strong host polyelectrolyte (HPE) when its charge density σ exceeds a critical value σ_C which increases with the ionic strength and decreases with the charge density of the HPE.[13] Upon further increase of the charge density, phase separation may occur at a concentration-dependent charge density σ_{PS}.[14] This has been demonstrated using mixed micelles of nonionic and ionic surfactants as polyions, applying turbidimetry. Fluorescence quenching (with labeled HPE) showed some transient binding even at $\sigma < \sigma_C$.[15] Dynamic light scattering (DLS) showed that aggregation of PECs grown to a critical size ∼45 nm took place when the turbidity increased sharply to a maximum and the electrophoretic mobility decreased to zero.[16] Interpolyelectrolyte complex (IPEC) formation of dendrimer GPEs with pH-dependent charge density was studied more recently by turbidimetry,[17] mainly motivated by the use of soluble IPECs with dendrimers or dendrimer−drug conjugates for biomedical applications.[18−20] Unlike association colloids from mixed surfactants, dendrimers are monodisperse and their size[21,22] is controlled by the synthesis. The star-branched internal architecture allows for a higher swelling in the periphery and a more diffuse distribution of charged groups, as has been shown by Monte Carlo simulations[23] and pH-dependent fluorescence study.[24] The dependence on the GPE charge density is almost the same as for systems with spherical GPEs[17] for the more spherelike dendrimers of higher generations. The polymer-enriched phase formed in the phase separation may either be a solid (flocculate) or a liquid (coacervate), where the latter is more likely for IPECs from weakly charged and hydrophilic polyelectrolytes. One interesting aspect is the ratio of "intramolecular" complexes (several GPE attached to a single HPE) to "intermolecular" complexes (containing more than one HPE). It is expected to scale with $C_{HPE}^{-5/4}$ and to increase with the GPE excess.[25] Equilibrium binding isotherms and static light-scattering (SLS) measurements[26] showed that at high excess of GPE micelles "intramolecular" complexes were predominant, where the repulsion between bound GPE stretches the HPE chain. Monte Carlo simulations have shown how the static and dynamic microstructure of an intramolecular IPEC depends on the polyelectrolyte flexibility. A flexible polyelectrolyte and a dendrimer mutually interpenetrate and the dendrimer can walk along the polyelectrolyte chain.[23] The structure of primary IPECs was proposed to be threads of HPE carrying separated or aggregated beads (dendrimer GPEs). The free parts (HPE loops, different beads) interact repulsive.[27]

Secondary aggregation of primary IPEC particles to form the precursors for the phase separation is known but scarcely studied. This colloid aggregation process might be influenced by the residual long-range potentials and could lead to structures different from the fractal clusters generated from uncharged

† Part of the special issue "International Symposium on Polyelectrolytes".

* To whom correspondence should be addressed. Tel: +81-52-789-5911; fax: +81-52-789-5912; e-mail: imae@nano.chem.nagoya-u.ac.jp.

10.1021/jp027365l CCC: $25.00
Published on Web 05/28/2003

colloids. The microstructure of coacervates[28] has not frequently been analyzed so far. Spongelike[29] and hierarchically self-assembled "fractal" networks[30] have been found by electron microscopy. In another case, a coacervate was found in the core of micelles, which were encapsulated in transient vesicles.[31]

In this paper, we study the structure of interpolyelectrolyte complexes (IPECs) formed between a rather flexible and homogeneously charged linear polyanion, a sodium poly(L-glutamate) with ~300 carboxylate groups, and a poly(amido amine) dendrimer of fourth generation (G4-PAMAM). Sixty-four primary amino groups in the periphery of this dendrimer become subsequently protonated and charged when the pH is lowered from 11 to 8, whereas 62 tertiary amino groups in the interior of the dendrimer require a pH lower than 7.5 to become protonated. In a similar system with poly(propylene imine) dendrimers, the protonation was facilitated when most protonated sites formed ion pairs with carboxylate groups of the polyelectrolyte.[27] The influence of the interaction on the polyelectrolyte behavior in this system will be the subject of a forthcoming paper. Here, we obtain the molecular weight and particle size of the IPEC from static and dynamic light-scattering data, as function of the proton activity. The aim is to follow the structural evolution of the IPEC from the interacting polyelectrolytes to the coacervate formed at higher proton activity and polymer concentration.

2. Theory

Free-Form (Indirect Fourier Transform) Method.[32] In a general approach, the scattering intensity $I(\mathbf{q})$, with $\mathbf{q}$ as the scattering vector, is the Fourier transform of the Patterson function $P(\mathbf{r})$

$$P(\mathbf{r}) = \int I(\mathbf{q}) \exp(-2\pi i \mathbf{qr}) d\mathbf{q},\ I(\mathbf{q}) = \int P(\mathbf{r}) \exp(2\pi i \mathbf{qr}) d\mathbf{r} \tag{1}$$

with $\mathbf{r}$ the real space coordinate. The Patterson function $P(\mathbf{r})$ is the self-convolution of the pair distribution function $\varphi(\mathbf{r})$ of the excess scattering length b, where $P(\mathbf{r}) = \varphi(\mathbf{r})^*\varphi(-\mathbf{r})$ with $\varphi(\mathbf{r}) = \sum b_i \delta(\mathbf{r} - \mathbf{r}_i)$ and δ is the Dirac delta function. For a large ensemble of randomly oriented particles, $\langle\varphi(\mathbf{r})\rangle_r$ becomes the scalar pair distance distribution function $p(r)$, which is related with the orientationally averaged correlation function $\gamma(r)$ of the excess scattering length: $p(r) = r^2\gamma(r)$. Accordingly, $I(q)$ instead of $I(\mathbf{q})$ can be transformed, where $q = (4\pi n/\lambda_0)\sin(\theta/2)$ is the scalar of the scattering vector $\mathbf{q}$, θ is the scalar of the scattering angle, n is the refractive index of the solution, and λ_0 is the wavelength of the incident radiation in a vacuum. By the "indirect Fourier transform" (IFT) method, proposed by Glatter[33] and developed by Svergun[34] and implemented in the GNOM program, a most stable and physically meaningful $p(r)$ function which would yield a scattering function very similar to the measured $I(q)$ is composed, regularized on the basis of the error estimates and some perceptive criteria.[35] Of importance are proper border conditions for $p(r)$, especially the constraint $p(r \geq d) = 0$ where d is the largest distance within a scattering particle in the ensemble. Because of this constraint, the method is inappropriate for large-domain periodic structures, since the resolution on the interval $0 \leq r \leq d$ is limited at least to the number of meaningful input data $I(q)$. Furthermore, if $p(r > \pi/q_{min})$ has to be evaluated, where q_{min} refers to the low-angle limit of the significant measured data, the reference $I(q < q_{min})$ must be extrapolated; this makes such data uncertain. From the fitted $p(r)$, the z-averaged radius of gyration R_g of the scattering mass is obtained as

$$R_g^2 = \frac{\int p(r) r^2 dr}{\int p(r) dr} \tag{2}$$

Scattering from Branched Particles. In this paper, we will fit scattering data with form factors $P_z(q)$ for homogeneously branched particles and polymer-micelle-like particles. The form factor of a homogeneously branched polydisperse polymer, with a z-averaged radius of gyration R_g of Gaussian chains between random branching points, is[36]

$$P_z(q) = [1 + (qR_g)^2/6]^{-2} \tag{3}$$

if the segment length is much smaller than the wavelength. Unlike the form factors for heterogeneously or starlike branched chains, the form factor does not depend on the number of interconnected chains. A hierarchically branched structure with two length scales for random branching could be described as the weighted sum of two terms of eq 3

$$P_z(q) = \phi_1[1 + (qR_{g,1})^2/6]^{-2} + (1 - \phi_1)[1 + (qR_{g,2})^2/6]^{-2} \tag{4}$$

where $R_{g,1}$ and $R_{g,2}$ are the R_g of Gaussian chains between random branching points of either class and ϕ_1 is a factor beween 0 and 1. A dispersed starlike structure with many bipolar chains originating from one self-assembled domain (e.g., a block copolymer micelle) has been described by a homogeneous sphere of radius R and excess scattering length b_S, with N_C Gaussian chains attached, each of these with a radius of gyration R_g and an excess scattering length b_C. The shape of its form factor[37,38] depends on the ratio b_S/b_C and thus on the relative scattering mass of the sphere (core) in comparison with that of the shell (corona) containing the attached chains.

Debye−Bueche Theory for Micro-Phase-Separated Gels. The scattering function $I(q)$ of a neutral gel with swelling pressure $\omega = \Pi_{mix} - G$, where Π_{mix} is the osmotic modulus and G is its shear modulus, can frequently be described as a sum of a dynamic (fast fluctuating) term $I_d(q)$ typical for the sol, too, and a static (very slowly fluctuating) term $I_s(q)$ describing the scattering from inhomogeneities produced in a microphase separation:[39]

$$I(q) = I_d(q) + I_s(q) \tag{5a}$$

where the dynamic term is (with φ as the solute volume fraction, ξ as the blob or mesh size, k_B as the Boltzmann constant, and T as the absolute temperature)

$$I_d(q) = \Delta\rho^2 \frac{k_B T \varphi^2}{\varphi \partial\omega/\partial\varphi + 4G/3} \cdot \frac{1}{1 + (q\xi)^2} \tag{5b}$$

and the static term is (with Ξ as the characteristic domain size of the concentration fluctuation and $\langle\Delta\varphi^2\rangle$ as its average amplitude)

$$I_s(q) = \Delta\rho^2 \frac{8\pi\Xi^3\langle\Delta\varphi^2\rangle}{[1 + (q\Xi)^2]^2} \tag{5c}$$

Both terms are proportional to the scattering contrast factor $\Delta\rho^2$ between solvent and solute. At given solute volume fraction φ, the contribution I_s of the static scattering mode increases

with the volume Ξ^3 of an inhomogeneity and with the solute density difference in the micro-phase-separated domains. Note the formal identity of the scattering functions eqs 3 and 5c when taking $R_g = 6^{1/2}\Xi$ because both types of density fluctuations are random.

Estimation of the Molecular Weight from Light Scattering. The general relation between the Rayleigh−Debye−Gans scattering and the molecular weight of homogeneous particles is

$$i_{excess}(q) = K_{Rayleigh} m M_w P_z(q) S(q) \tag{6}$$

with $i_{excess}(q)$ as the Rayleigh ratio of the solute, m as its mass concentration, M_w as its weight-averaged molecular weight, and $P_z(q)$ and $S(q)$ as the z-averaged structure factors for decoupled intra- and interparticle interference, respectively; $K_{Rayleigh} = 4\pi^2 n_0^2 (dn/dm)^2/(N_A \lambda_0^4)$ is the Rayleigh constant where n and n_0 are the refractive indices of the solution and of the solvent, respectively, and dn/dm is the weight-averaged refractive index increment of the (interacting) solute.[40] $P_z(q)S(q)$ can be obtained from model fitting to the scattering function where generally $S(q)$ tends to values close to 1 at large q in absence of short-range positional order, and $P_z(q = 0) = 1$.

3. Experimental Section

Materials. The amino-terminated poly(amido amine) dendrimer of fourth generation (G4-PAMAM dendrimer, M_w = 14.215 kg/mol) was supplied from Aldrich, as 10% solution in methanol. Sodium poly(L-glutamate) (NaPGA, M_w ∼45 kg/mol) was supplied from Peptide Institute Inc., lot 350922. Sodium chloride (NaCl) was analytical grade. Water was distilled and further purified by a Millipore Milli-Q apparatus. Aqueous solutions of hydrochloric acid (0.25 M HCl) and sodium hydroxide (NaOH) were prepared from Wako normal solutions.

Sample Preparation. Methanol was evaporated from the dendrimer solution in a vacuum (∼0.1 mbar). NaPGA was dried in a vacuum over silica gel. Stock solutions of the individual polymers (10 and 2 mg/cm^3 PAMAM dendrimer, 1 and 0.2 mg/cm^3 NaPGA) in aqueous 0.25 M NaCl and of the solvent (aqueous 0.25 M NaCl) were gently filtered through 0.22 μm Durapore membranes (Millipore Millex GV), stored at 4−8 °C, and mixed for sample preparation by weighing.

Methods. All measurements were performed at 25 ± 1 °C. Hamilton syringes (50 mm^3) were used for titrations. The pH was detected by a combined glass electrode (Iwaki, 4 mm ∅). Its calibration was checked by standard buffers before and after the titration. Measured pH was corrected by a drift of the offset (EMF at pH 6.95) of up to the equivalent of 0.15 pH units which was taken as linear with the number of HCl additions, whereas the slope (dEMF/dpH) remained always unchanged.

Static (SLS) and dynamic (DLS) light scattering was measured from cylindrical cuvettes (10 mm ∅), using a light-scattering photometer DLS-700 from Otsuka Electronics, equipped with a 15 mW argon ion laser operating at a wavelength λ_0 = 488 nm. For SLS, the average intensities of three to four measurements per angle (with different cuvette rotational positions) were corrected for the solvent contribution and normalized to absolute intensities (Rayleigh ratios) of the solute contribution (i_{excess}) by means of a standard (benzene) and the Herman−Lewinson correction of the scattering volume at different refractive indices.

For DLS, homodyne intensity autocorrelation functions in the time domain (TCFs) from a fixed scattering volume were sampled for 300−600 s by an ALV-5000 correlator and analyzed by the Contin method to obtain the amplitude spectrum $A(\tau)$ of exponential decay modes in the field correlation function $g_1(t) = \int A(\tau)\exp(-t/\tau)$ where t is the lag time. Peaks of $A(\log \tau)$ were integrated and their weight-averaged relaxation times τ_i converted to the diffusivities $D_i(q) = (\tau_i q^2)^{-1}$ and to the apparent correlation lengths $\xi_{app,i}(q) = k_B T/(6\pi\eta_s D_i(q))$, where η_s is the solvent viscosity.

Small-angle X-ray scattering (SAXS) measurements were performed with a Rigaku three-slit pinhole camera, equipped with a Rigaku ultraX18HB X-ray source (operated at 45 kV, 80 mA), He-protected Osmic CMF25-77.5Cu6 confocal multilayer optics, 0.5 and 0.4 mm pinholes, and a Fuji image plate (IP) 2D-detector placed at a distance of 1000 mm from the sample. The average wavelength (Cu−$K_{\alpha 1,2}$) was λ_0 = 0.1541 nm, and the beam divergence had a full width at half-maximum (fwhm) of Δq = 0.034 nm^{-1} at the detector. Samples were sealed as ∼2-mm-thick (∼1 mm in coacervates) slabs between two 7.5-μm-thick Kapton films and exposed for 22 h. The scanned patterns were azimuthally averaged and corrected for the background (water between Kapton films), to obtain the scattering function $i_{excess}(q)$ of the solute on arbitrary scale.

4. Results and Discussion

Inter-polyelectrolyte complex (IPEC) formation upon partial protonation of the G4-PAMAM dendrimer (guest polyelectrolyte, GPE) by HCl addition to the aqueous solution was studied for two concentrations of the NaPGA (host polyelectrolyte, HPE): 0.2 mg/cm^3 and 1 mg/cm^3. The carboxylate groups remain to more than 99% dissociated at pH >7.5.[41,42] Initially, 0.25 M NaOH was added to obtain a pH between 10.5 and 11 at which the dendrimer is not yet a polycation.

Mixtures with different excess Φ of the total number of dendrimer basic amino groups (N(GPE) = 126 per GPE) over the total number of carboxylate groups (N(HPE) = 298 per HPE) were studied,

$$\Phi = \frac{m(\mathrm{GPE})}{m(\mathrm{HPE})} \cdot \frac{M(\mathrm{HPE})/N(\mathrm{HPE})}{M(\mathrm{GPE})/N(\mathrm{GPE})} \tag{7}$$

where m is the mass concentration, M is the molecular weight, and N is the degree of polymerization or the number of functional groups per polymer molecule. The concentrations of the independent polyelectrolytes were always below the corresponding overlap concentrations C^*. However, the overlap condition may be reached even with a few HPE·GPE·HPE cross-links of (transient) IPECs, and some remaining Coulomb interactions must be considered.

Static Light Scattering. The evolution of the scattering intensity with the pH decrease, thus protonation and charging of the dendrimer GPE, was observed in the q range from 9 to 33 μm^{-1} for the more dilute systems (Figure 1) and in the slightly extended q range from 3 to 33 μm^{-1} in the higher HPE concentration.

In Figure 1, the scattering from the dispersed colloids $i_{excess}(q)$ is shown on double-logarithmic scale. For q < 30 μm^{-1}, the scattering function can be approximated by the scattering from fractals with fractal dimension d_m, obtained as the negative slope $-\Delta\log(i_{excess})/\Delta\log(q)$ and plotted in Figure 2. For both the system with GPE excess (Φ = 2.67) and the stoichiometric mixture (Φ = 1.01), the evolution of d_m with the pH can be divided into three stages. In the first stage (pH >9.5), d_m increases from 1.2 to 1.6. From pH 9.5 to 8.8, d_m increases to ∼4.0 (second stage) and remains at values between 3.5 and 4 upon further acidification up to pH 5 (third stage). d_m values

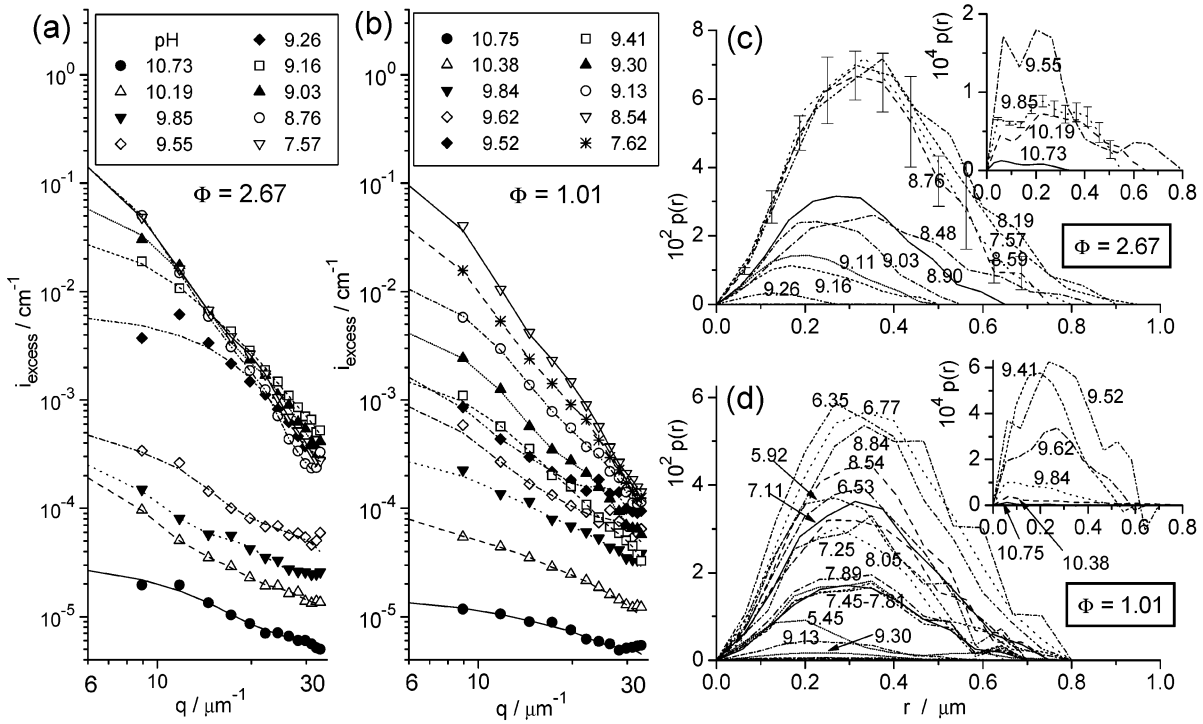

Figure 1. SLS scattering functions for 0.2 mg/cm^3 NaPGA with (a) 0.4·mg/cm^3, (b) 0.15·mg/cm^3 G4-PAMAM dendrimer, as a function of the pH. Lines are regularized IFT fits; the corresponding pair distance distribution functions are shown in (c) and (d), respectively, labeled with the pH.

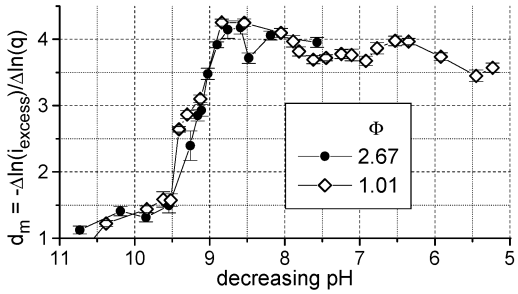

Figure 2. Apparent fractal dimensions d_m from the slopes of linear fits to the data in Figure 1a and b. All lines are guides for the eye.

far below 1.7 likely describe scattering from strongly self-avoiding wormlike chains or even extended coils (first stage). On the other side of the transition, d_m values ≥3.6 likely describe the scattering of large homogeneous objects with rather smooth surfaces (surface fractals, third stage).

However, additional nonfractal motifs can be seen in the scattering functions: (i) a broad shoulder at $q_m \sim 20\ \mu m^{-1}$, predominantly developing at pH <9, which could indicate a weak interparticle correlation length of $2\pi/q_m \sim 300$ nm; (ii) an upturn at $q > 30\ \mu m^{-1}$ ($\theta > 135°$) which could be due to a systematic error, namely, a parasatic small-angle scattered reflection of the transmitted beam from the opposite sample/cuvette interface. These values were not included for the curve fitting in Figure 1.

To extrapolate the forward scattering intensity at $q = 0$ and to find a valid estimate for the R_g, the Guinier method could not be applied because qR_g was not <0.1. The free-form method was thus applied throughout. The IFT was performed with the program GNOM (V. 4.3) from the EMBL, Hamburg, Germany. Fits are displayed in Figure 1, together with the corresponding pair distance distribution functions $p(r)$. The fits generally reproduce the intermediate "shoulder" at $q \sim 20\ \mu m^{-1}$.

The size of the scattering inhomogeneities (Figure 3a) was obtained as z-averaged R_g parameter with eq 2 from the $p(r)$ in Figure 1c, d and as Ξ parameter with eq 5 from Debye−Bueche (DB) fits, which were most acceptable at pH >9 (fits not shown, but see error bars). At pH <9, the DB fits suffered from a strong linear dependency between the Ξ and I_S parameters. Roughly, the size of scattering inhomogeneities scales with the proton activity with an exponent 0.44 (11 > pH > 8.8), whereas it remains constant at $R_g \sim 250$ nm at pH <9.

The absolute intensities at zero scattering angle (Figure 3b), which might be overestimated by up to one decade in DB fits, permit to estimate the M_w (right scale in Figure 3b); it was calculated from the intensities with eq 6 and an estimated $dn/dm = 0.16$ cm^3 g^{-1} for the interacting IPEC particles. From pH 10.8 to 8.8, M_w increases by just 4 orders of magnitude (IFT fit results). The stages of the evolution become more apparent, in which the M_w seems to scale with the proton activity with the scaling exponents 2 (pH 11 to 10, first stage), 1 (pH 10 to 9.5, still first stage), 3 (pH 9.5 to 8.9, second stage), and 0 (pH 8.8 to 6, third stage), respectively. The extrapolations with the poorer DB fits yield systematically overestimated M_w when also Ξ is overestimated because of the linear dependence of the fitting parameters. The estimated M_w and the theoretical M_w for noninteracting polymers at $\Phi = 1.01$ (31800 g/mol) agree well at pH 10.7. At the onset of the second stage (pH 9.5), M_w has increased to 10^6 g/mol, which would correspond to multimolecular IPECs $(HPE_1GPE_{2.38})_{12.7}$ (in the monodisperse case). The maximum M_w in the third stage (3×10^8 g/mol) would correspond to IPECs $(HPE_1GPE_{2.38})_{3800}$ (in the monodisperse case). However, it is likely that the inhomogeneities in the refractive index are partly due to an inhomogeneous distribution of the small ions. NaCl has a $dn/dm = 0.175$ cm^3/g in aqueous solution at $C = 0.25$ M ($m = 14.61$ mg/cm^3),[43] mainly because of the highly polarizable Cl^- anions. When dendrimer polycations get attracted by the residual electric field of the HPE, the IPEC may contain an HPE core and a first shell with excess GPE polycations cross-linked or not by the former. Each polycation carries an ionic cloud enriched in Cl^- ions so that a second diffuse shell, enriched in Cl^- ions, will

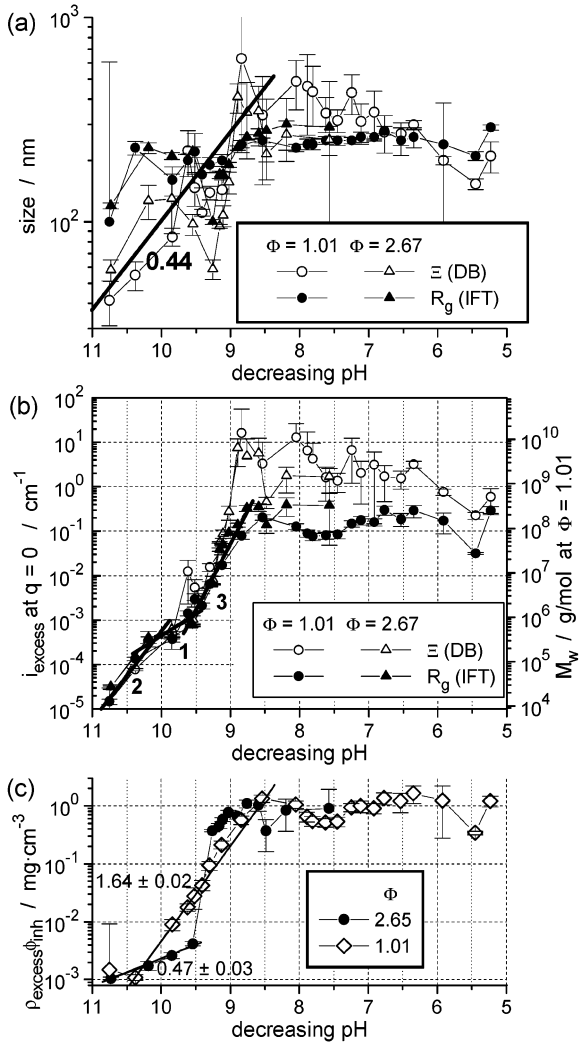

Figure 3. From fits to the data in Figure 1: (a) *z*-averaged R_g obtained from the $p(r)$ and characteristic sizes Ξ of "static" inhomogeneities from Debye−Bueche (DB) fits (not shown); (b) zero-angle scattering intensities from IFT and DB fits, the right scale indicating M_w estimates for the $\Phi = 1.01$ case according to eq 6; (c) excess polymer density in the inhomogeneities (when considered as homogeneous spheres), calculated from the IFT fit results for M_w and R_g. Some possible scaling regimes are indicated by thick straight lines labeled with their slopes.

circumfere the interacting polyelectrolytes. The M_w of the IPEC includes the scattering mass of this ionic cloud, its Cl^- excess density being largest when the IPEC is considerably overcharged. Fivefold overcharging has been reported in some case and the theoretical limit is under discussion, so far considered to be much smaller.[44]

The excess mass density ρ_{excess} of the solute in an average inhomogeneity can be estimated as $\rho_{excess}\phi_{P,inhom} = M_w/V_{inhom}$ where $V_{inhom} = (4\pi/3)(5/3)^{3/2}R_g^3$ is its volume considered to be spherical and $\phi_{P,inhom}$ is the probability to find the polymer inside the inhomogeneities. $\phi_{P,inhom}$ can be assumed to be unity in the third stage when apparently all the scattering comes from the large inhomogeneities. Figure 3c shows that around the transition with a threshold at pH ∼9.5, the product $\rho_{excess}\phi_{P,inhom}$ increases with the proton activity in a power-law fashion and saturates at an excess polymer density of ∼2 mg/cm^3 after the transition. The inhomogeneities thus contain more than 99% of solvent even after the transition. The transition is smooth in the stoichiometric case (power exponent 1.64 ± 0.02 over two decades) but is not so with dendrimer excess, where the power-law (exponent 0.47 ± 0.03) brakes at around the threshold from the first to the second stage.

Some information on the density distribution in the inhomogeneities can be obtained from the pair distance distribution functions. In the shape analysis of the $p(r)$, we have to be aware that the total function is a superimposition of the scattering mass weighted pair distance distribution functions of all present scattering domains. The relation between a particle's shape and its $p(r)$ is described in ref 45 for several shapes; generally, it becomes zero for $r > d$ where d is the largest particle diameter. A homogeneous sphere with outer shell radius R has a $p(r)$ with a right-tilted bell shape, with a maximum at $r = 1.05\,R$. A denser core with a less dense shell (e.g., a star polymer or a Gaussian chain) provides a $p(r)$ roughly similar to a log-normal distribution, with the maximum shifted to $r < R$. For a long cylinder particle, $p(r)$ would exhibit a maximum at the diameter of the cylinder cross-section and a long tail. The shape of $p(r)$ at pH ∼10.5 may correspond to such a cylinder-shaped particle (with a cross-section of ∼50 nm). But at pH 10.2 and below, $p(r)$ becomes clearly bimodal. Toward pH ∼9.5 (end of first stage), the scattering from the smaller mode ($r_{max} \sim 60$ nm) increases by at least a factor of 10, and then the second mode ($r_{max} \sim 270$ nm) becomes dominant. Toward pH 8.5, the $p(r)$ expands to 90% of its "final" extension and assumes a distorted bell shape with its maximum at $r \sim 320$ nm and a pronounced tail which reaches up to $r = 800$ nm. The shape of $p(r)$ does not change further when the pH is lowered from 8.5 to 7.5 (third stage). The evolution of the scattering beyond pH 7.5 was only studied for the stoichiometric case ($\Phi = 1.01$). Until pH 6, there is no major change. After that, toward pH 5.45 the maximum of $p(r)$ decreases to 190 nm and the scattering intensity decreases by a factor of 7, whereas the shape of $p(r)$ remains virtually unchanged.

The small mode ($r_{max} \sim 60$ nm) likely corresponds to the scattering from elongated polyanions and "primary" IPEC particles and their counterion clouds. The large mode then corresponds to multimolecular "secondary" IPECs and their ionic clouds. In the second stage, both types of IPEC coexist. All particles become less dense in their periphery.

Figure 4 shows some scattering curves from mixtures with a 5-fold increased polymer concentration (1 mg/cm^3 NaPGA) and different excess of the GPE upon HCl addition. The measurement at the last pH (∼9) of a series corresponds to the scattering of the transparent upper phase over a minority coacervate phase (<2 vol %) which started to separate at a pH just above and sedimented within 3 h at normal gravity. Zero-angle scattering intensities and *z*-averaged R_g from IFT fits are reported in Table 1. The insets of Figure 4a−c show alternative DB fits (eq 5), with their parameters also listed in Table 1. Scattering curves which were well fitted by the DB model were obtained only when the $p(r)$ looked nicely bimodal, for example, for $\Phi = 13.3$ at the two highest pH. In those cases the "dynamic" contribution was from a polymer liquid with a correlation length $\xi \sim 45 \pm 20$ nm. In all cases when the DB fit seemed not quite inappropriate, Ξ was in the range between 130 and 800 nm and was less correlated with the pH than in the more dilute systems.The *z*-averaged R_g found from the IFT fits (110−830 nm, Table 1) usually increase when the pH is decreased, and correlations of the excess scattering length density reach to a distance of 2 μm.

The extrapolated scattering intensities at zero angle are also much less correlated with the pH than as observed in the dilute systems. Values between 1.5×10^{-5} cm^{-1} and 0.05 cm^{-1} are found from the IFT fits between pH ∼10 and 9, spanning 3.5

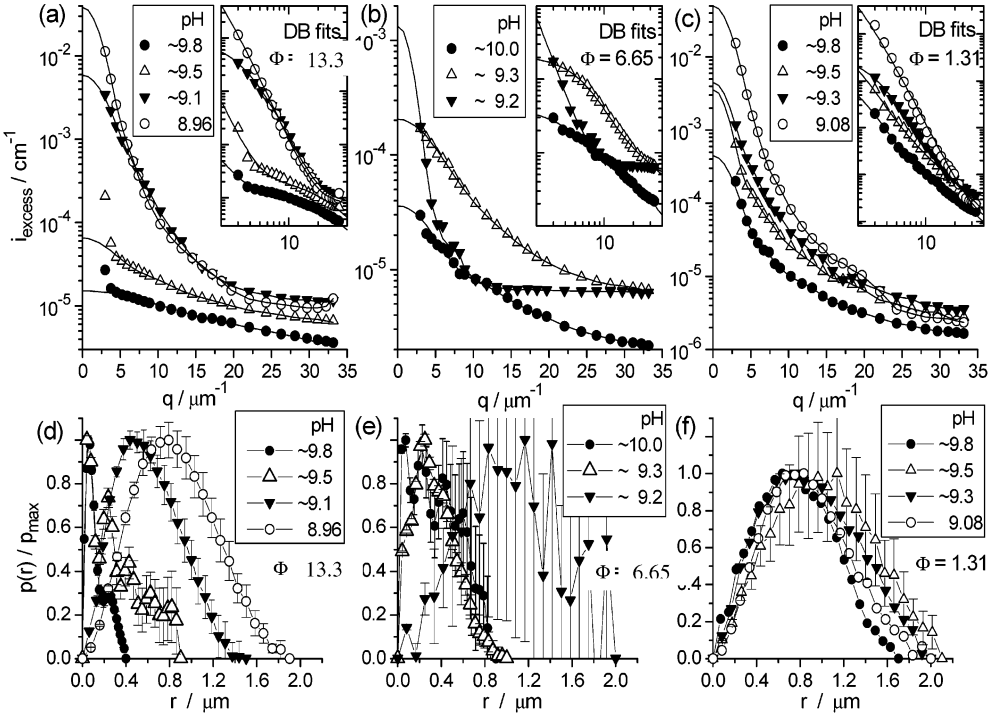

Figure 4. SLS from 1 mg/cm^3 NaPGA + (a) 10, (b) 5, (c) 1 mg/cm^3 G4-PAMAM dendrimer, as a function of the pH. Lines represent IFTs of the $p(r)$ displayed in (d−f), respectively. The inserts show DB fits (eq 5) to the data on double-logarithmic scale.

TABLE 1: IFT (columns 3, 4) and DB Fitting Results (eq 5, column 5) for Systems with 1 mg/cm^3 NaPGA

Φ	pH	R_g/nm	$i_{excess}(q=0)$ 10^5 cm^{-1}	Ξ/nm
13.3	∼9.8	110 ± 10	1.52 ± 0.04	620 ± 270
13.3	∼9.5	290 ± 30	6.5 ± 0.7	1600 ± 4400
13.3	∼9.1	470 ± 30	590 ± 60	270 ± 10
13.3	8.96	650 ± 20	3800 ± 400	830 ± 50
6.65	∼10.0	310 ± 40	6.2 ± 1.5	180 ± 30
6.65	∼9.3	270 ± 20	21 ± 1	130 ± 10
6.65	∼9.2	340 ± 120	6.7 ± 2.2	1100 ± 400
1.31	∼9.8	590 ± 120	45 ± 20	520 ± 60
1.31	∼9.5	780 ± 40	360 ± 110	620 ± 200
1.31	∼9.3	700 ± 110	450 ± 160	310 ± 20
1.31	9.08	670 ± 40	5000 ± 1100	740 ± 240

decades. This is well comparable to the 4 decades between pH 10.5 and 8.8 or the 3 decades between pH 10 and 8.8 found for the more dilute systems. The plateau maximum in the dilute systems (∼0.2 cm^{-1}) is 4 times stronger than for the 5-fold more polymer-containing systems. This holds also if we compare the less confident DB results. Apparently, the attained polymer density in the fluctuations is less different from the average polymer density than in the more dilute system, where the same density provides a higher excess density. The scattering intensity is proportional to the squared excess density $\langle\Delta\varphi^2\rangle$ (eq 4b).

Dynamic Light Scattering (DLS). For the dilute systems with 0.2 mg/cm^3 NaPGA, in Figure 5 we report the pH dependence of the distribution of the apparent correlation lengths ξ_{app} taken from DLS measurements at $\theta = 30°$ ($q = 8.9\ \mu m^{-1}$).

Two dynamic modes are clearly resolved in the Contin decomposed spectra of relaxation times: a fast mode starting at pH 11 with correlation length $\xi_{app,2} = 10^{1.9} = 80$ nm, a medium mode starting at $\xi_{app,m} = 10^{3.5} = 3200$ nm, and a slow mode with a relaxation time $\tau_3 \sim 5$ s (corresponding to an apparent correlation length of 10^5 nm). Two transitions are clearly observed, the first between pH 9.3 and 9. Starting from pH 11 with $\xi_{app,2} = 10^{1.9} = 80$ nm, toward this transition the fast mode slows down to reach $\xi_{app,2}$ values of $10^{3.1} = 1300$ nm (at $\Phi = 2.67$) and $10^{2.8} = 630$ nm (at $\Phi = 1.01$),

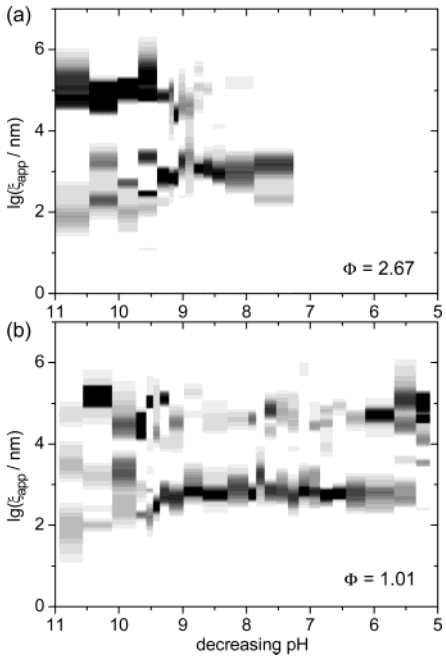

Figure 5. Apparent correlation lengths from Contin fits to TCFs obtained at 30° scattering angle, from 0.2 mg/cm^3 NaPGA, with (a) 0.4 mg/cm^3 and (b) 0.15 mg/cm^3 G4-PAMAM dendrimer. The intensity of the dark shading is proportional to the g_1 amplitude $A(\xi_{app} \propto \tau)$.

respectively. The medium mode with $\xi_{app,m} = 10^{3.5} = 3200$ nm at pH 10.7 disappears at the transition or merges with the faster component. The most apparent change in the transition is the strong decrease of the *relative* scattering amplitude of the slow mode: the fast mode becomes the dominant one in the dynamic structure factor between pH 9 and 6.2. In this entire region, there is no change in the mode's frequency. Upon acidifying the stoichiometric IPEC mixture ($\Phi = 1.01$) further, the slow mode, with maintained $\tau_3 = 5$ s, becomes dominant again.

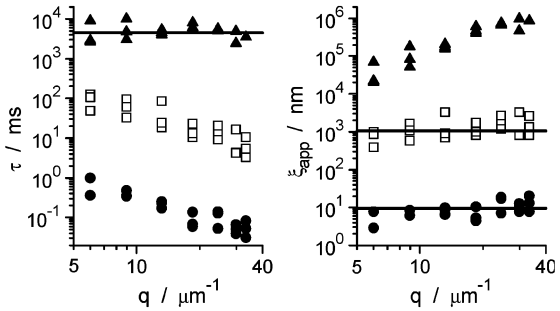

Figure 6. Example of angle dependence of modes in the Contin inverted TCFs, from 1 mg/cm^3 NaPGA with 10 mg/cm^3 PAMAM dendrimer ($\Phi = 13.4$). (●) fast mode (dendrimer diffusion); (□) second mode (IPEC diffusion); (▲) third mode (network relaxation time: "static" inhomogeneity fluctuations).

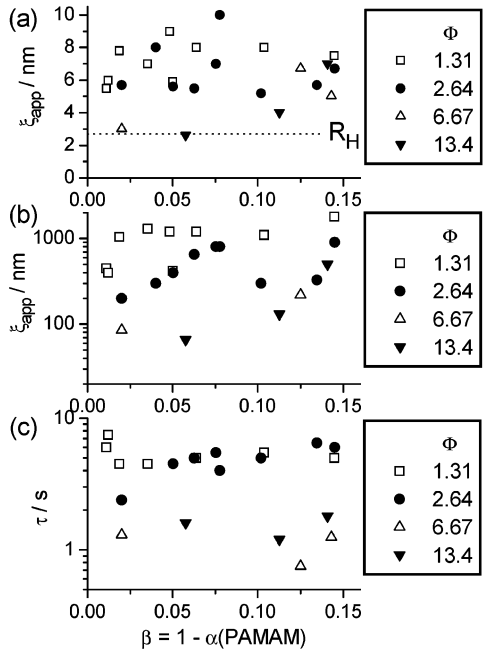

Figure 7. Scattering-angle averaged relaxation modes and the corresponding apparent correlation lengths from Contin fits to TCFs, from 1 mg/cm^3 NaPGA, with 1−10 mg/cm^3 G4-PAMAM dendrimer. (a) fast mode (dendrimer diffusion); (b) second mode (IPEC diffusion); (c) third mode (network relaxation time).

With the higher polymer concentration (1 mg/cm^3 NaPGA), we measured the q dependence of the dynamic structure factor at different Φ at pH 9.7 ± 0.2. Figure 6 shows the series with the highest dendrimer excess ($\Phi = 13.3$).

Two fast "diffusive" modes can be clearly distinguished, separated by 2 orders of magnitude. The faster component appears with a q-averaged $\xi_{app,1} \sim 10^{0.9} = 7.9$ nm, and the more intense slower component with $\xi_{app,2} \sim 10^{3.1} = 1300$ nm. The ξ_{app} of both components increases considerably and is well correlated with the q value; at zero q they would extrapolate to $\xi_{app,1} \sim 10^{0.6} = 4.0$ nm and $\xi_{app,2} \sim 10^{2.7} = 500$ nm, respectively.

In Figure 7, we show the dependence of the modes' frequencies on the dendrimer excess and on the degree of protonation (β) of the dendrimer, which was calculated from the added amount of HCl with the help of the potentiometric titration curve of the dendrimer to be reported elsewhere. The explored range corresponds to pH between 10 and 9.3. The fastest mode was detected usually with a $\xi_{app,1} \sim 6$ nm (Figure 7a). It was detected somewhat faster only for the highest dendrimer excesses at low degree of dendrimer protonation. In these cases, it came close to the reported hydrodynamic radius $R_H = 2.66$ nm of the dendrimer in water at pH 8,[46] which is indicated as dashed line. The more intense second mode (Figure 7b) was more dependent on the varied parameters. However, in the nearly stoichiometric case ($\Phi = 1.31$), the maximum value $\xi_{app,2} \sim 1000$ nm was reached upon only a slight HCl addition; in the high dendrimer excess ($\Phi = 6.67$ and 13.3), a lower pH was required to let the $\xi_{app,2}$ rise from ∼60 nm to 400 nm.

The slow mode's relaxation time (Figure 7c) was independent of the dendrimer protonation but was 4 times slower for the lower dendrimer excesses ($\Phi = 1.31$ and 2.67), where $\tau_3 \sim 5$ s.

Assignment of Modes in DLS and Comparison with SLS. The fastest mode with $\xi_{app,1} \sim 6$ nm obviously corresponds to the diffusion of dendrimers. This diffusion is slowed by transient binding to slower moving polyanions, as the dendrimer becomes protonated.

The mode starting at $\xi_{app,2} = 10^{1.9} = 80$ nm provides a measure of the correlation length ξ between homogeneously distributed, repulsive interacting polyanions or IPECs. From the cell volume $V_{cell} = (4\pi/3)(\xi/2)^3$ and the average HPE polyanion number density, the aggregation number of the IPEC can be obtained in the monodisperse case as $N_{agg,HPE} = N_A V_{cell} m_{HPE}/M_{HPE}$ at $m_{HPE} = 0.2$ mg/cm^3; thus one obtains $N_{agg,HPE} = 1$ at $\xi = 89$ nm and $N_{agg,HPE} = 1401$ at $\xi = 10^3$ nm, corresponding to $M_w = 1.1 \times 10^8$ g/mol for the stoichiometric IPEC $(HPE_1\text{-}GPE_{2.38})_{1401}$. The observed range of $\xi_{app,2}$ thus exactly spans the evolution from the monomolecular IPECs at pH 10.7 to the saturated IPECs at pH 8.8, for which $M_w = 2 \times 10^8$ g/mol has been found from SLS.

The medium mode starting at $\xi_{app,m} = 10^{3.5} = 3200$ nm was not observed systematically and could be due to dust or a noise-handling problem of the Contin regularization (an artifact).

The nondiffusive slow mode[47,48] with a relaxation time $\tau_3 \sim 5$ s corresponds to the network relaxation time, $\tau_3 \sim \tau_R = (D_g q_g^2)^{-1}$ where $D_g \sim D_1 = k_B T/(6\pi\eta_s\xi_1) \sim 2.4 \times 10^{-9}$ cm^{2}s^{-1} is the gel diffusion coefficient obtained from the asymptotic high-q plateau of the fast mode (whereas the cooperative diffusion coefficient D_c can be obtained from the zero-q extrapolation of this mode) and q_g^{-1} is a characteristic length describing the radius of action of the elastic force coupling in the transient gel (related with the damping by viscous drag forces); here, it can be evaluated to $q_g^{-1} \sim 1.1$ μm. Interestingly, q_g^{-1} equals the limiting size of $\xi_{app,2}$ (within precision of the estimation); the IPECs at the plateau size are still weakly interacting with their neighbors, whereas homogeneously distributed ones of larger sizes would be screened from each other. The elastic interaction is probably mediated by long-range electrostatic coupling (osmotic depletion interaction between ionic clouds) and not by mechanical cross-links between so distant IPECs.

SAXS from the Water-Rich Phase. In Figure 8, the SAXS scattering functions from the IPEC solution of 1 mg/cm^3 NaPGA and 10 mg/cm^3 G4-PAMAM are shown as a function of the pH. All functions obtained in the region pH >9.3, that is, before the phase separation was reached, are very similar. They show a strong upturn at $q < 0.2$ nm^{-1} and a smooth nearly-exponential decay of $I_{excess}(q)$ at $q > 0.25$ nm^{-1}. In the double-logarithmic representation (not shown), the low-q upturn exhibits a power-law decay with $I(q) \propto q^{-6}$ in the short range 0.15 nm$^{-1} < q <$ 0.2 nm^{-1}; the excess intensity measured in this q range was at least 5 times higher than that from the entire background.

The scaling $I(q) \propto q^{-6}$ is typical for the scattering from a critical spinodal structure,[49] in the range $1 < q/q_m < 2.5$ where

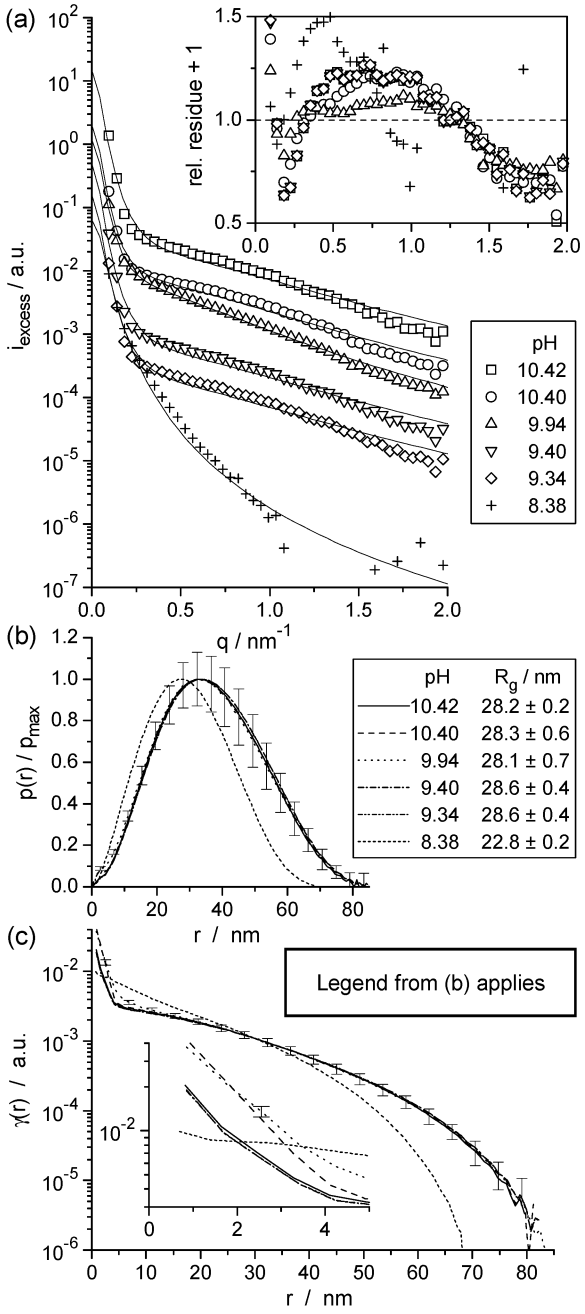

Figure 8. SAXS from 1 mg/cm^3 NaPGA and 10 mg/cm^3 G4-PAMAM at different pH. The last curve (pH 8.38) corresponds to the upper phase after phase separation. (a) Scattering functions, each shifted by a factor of one-third with respect to the former, and fits to a hierarchical branched model (eq 4); (b) normalized pair distance distribution functions, and (c) characteristic pair correlation functions from IFT fits, with a typical set of error bars.

q_m is the position of the structure factor maximum. The only other possibility to find such a strong decay in absence of Bragg reflections is the vicinity of a form factor minimum; in the actual case there could be one at $q = 0.2$ nm^{-1}. We also find the asymptotic behavior $I_{excess}(q) \propto q^{-3}$, in the range 1 nm^{-1} < q < 2 nm^{-1}. Its proper assignment may have suffered from systematically wrong background subtraction. However, for a dendrimer with a smoother surface than that of a Gaussian coil, we would even expect a faster decaying scattering function. We therefore fitted the scattering function to a hierarchically branched model (eq 4) equivalent to a randomly branched gel (eq 3) with random larger-scale inhomogeneities (eq 5c). The fitting results are displayed in Table 2. The chain segments between branching points have an $R_g = 2.3 \pm 0.2$ nm, which is $2.5^{1/3}$ larger than the R_g of a dendrimer (1.7 nm); the structural unit likely is a dendrimer bead on a chain of HPE between two other beads. In the upper phase over the coacervate at pH 8.4, the feature is missing. The low-q upturn hints to inhomogeneities with an R_g of ~44 nm in the single-phase region. However, the whole model does not provide a correct fit to the data, as can be seen in the residues plot.

TABLE 2: Hierarchically Branched Chain Model (Eq 4) Fitting Parameters for SAXS Data of IPEC Solutions at $\Phi = 13.3$ (Fits in Figure 8a)

pH	$R_{g,1}$/nm	$R_{g,2}$/nm[a]	ϕ_1^{-1} [a]	$[(4\pi/3)\phi_1^{-1}]^{1/3}$	$R_{g,IFT}$/nm
10.42	2.14 ± 0.07	≥44	≥680	≥14	28.2 ± 0.2
10.4	2.31 ± 0.04	≥44	≥260	≥10	28.3 ± 0.6
9.94	2.96 ± 0.03	≥42	≥180	≥ 9	28.1 ± 0.7
9.40	2.14 ± 0.06	≥47	≥790	≥15	28.6 ± 0.4
9.34	2.15 ± 0.06	≥46	≥780	≥15	28.6 ± 0.4
8.38		≥34			22.8 ± 0.2

[a] Minimum values of highly linear dependent. ϕ_1^{-1}, $R_{g,2}$ which can fit the data.

Lacking a better model, we applied the IFT method and look at the resulting pair distance distribution fucnctions (Figure 8b) and the related characteristic functions $\gamma(r)$ (Figure 8c). All the scattering from the homogeneous gel is represented by the small shoulder of $p(r)$ between $r = 0$ and 5 nm and the corresponding decay mode in $\gamma(r)$. It is missing at pH 8.38, after the coacervate has settled down. The large rest of the $p(r)$ function describes the correlations in the gel inhomogeneities. The clearly asymmetric bell shape of $p(r)$ indicates that these inhomogeneities with $R_g = 28.4 \pm 0.2$ nm have a denser core and a less dense corona. Only a smaller cutoff of these likely polydisperse (sub) particles remains in the solution over the coacervate phase at pH 8.38; the R_g shrunk to 22.8 ± 0.2 nm but the shape of $p(r)$ remained unchanged except for the missing shoulder.

SAXS from the Polymer-Rich Phase (Coacervate). Upon acidification to pH ~9, a slightly hazy and viscous liquid was sedimented from the mixtures containing 1 mg/cm^3 NaPGA and excess dendrimer. It proved to be optically isotropic (no patterns were seen between crossed polarizers).

The SAXS curves in Figure 9 show inner and intermediate parts of the scattering functions which look very similar to those in Figure 8. Unfortunately, we cannot determine with any confidence the asymptotic behavior in the outer part because of a problem with an uneven background. Another problem was the small quantity of the coacervate; we are not sure that the beam always passed only through the coacervate phase (a 2−3-mm-thickness layer in the sample). One notes that the second pattern (at $\Phi = 6.65$) is different from the others: it yields a well-resolved peak at $r = 2.4$ nm in the pair distance distribution function and shows a less pronounced upturn of the scattering function at low q. The integrated R_g of the inhomogeneities, responsible for the low-q upturns, are 18 ± 2 nm, significantly smaller than for the mixtures at pH above the phase separation transition and even smaller than the one in the upper phase at pH 8.38. Fits to the hierarchically branched model (eq 4) yield inhomogeneities with $R_g = 41 \pm 3$ nm and for the segments between branching points of the small network R_g values increasing from 2.47 to 3.02 nm when the dendrimer excess is decreased from 13.4 to 1.33 (see Table 3). However, the fits again fail to reproduce the low-q upturn properly.

The scattering function of the coacervate from the near-stoichiometric mixture ($\Phi = 1.33$) looks very similar to that of a copolymer micelle with strong excluded-volume interaction.

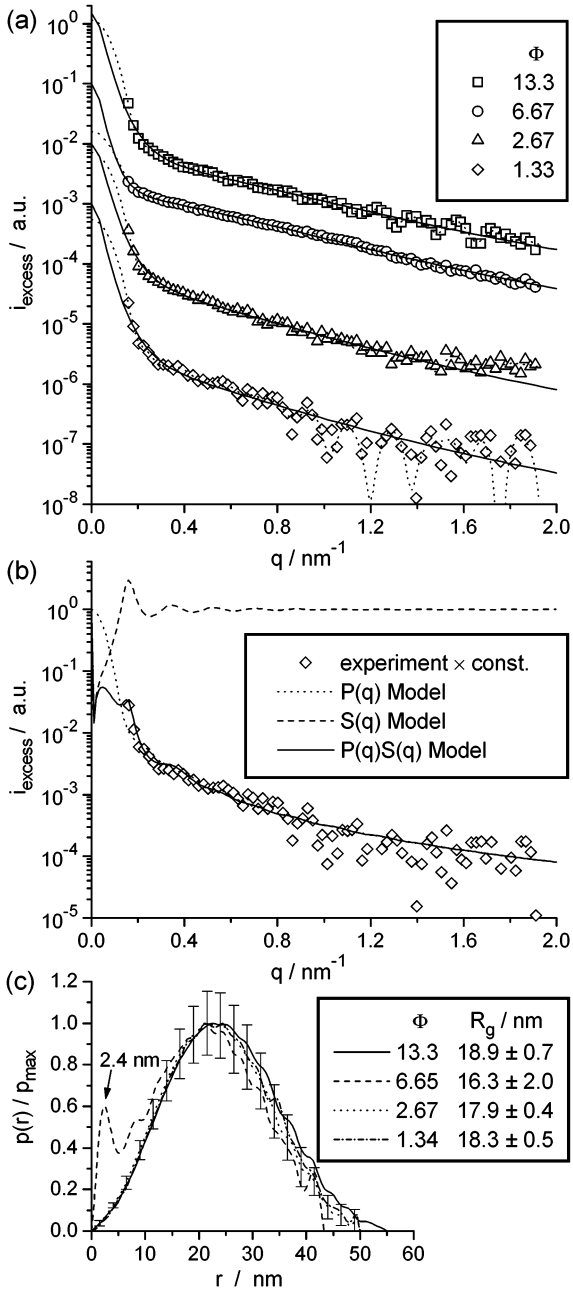

Figure 9. SAXS from coacervates at pH ~8.8 in systems with 1 mg/cm^3 NaPGA and variable dendrimer excess. (a) logarithmic plot (each curve shifted by one decade), with fits to hierarchically branched model (eq 4); (b) a no-optimized fit of the model of copolymer micelles (form factor $P(q)$[37,38]) with hard sphere excluded volume interaction (structure factor $S(q)$[38]) to the data at $\Phi = 1.33$, with the parameters $R_{HS} = 35$ nm, $R = 16$ nm, $R_{g,chain} = 10$ nm, $N_C = 40$, $\phi_{HS} = 0.25$, $\phi_{core} = 0.024$, $\rho_S/\rho_C = 10$; (c) normalized distance distribution functions from IFT fits.

A comparison with such a model is shown in Figure 9b. The form factor[37,38] $P(q)$ is for a sphere with radius $R = 16$ nm and $N_C = 40$ attached Gaussian chains with radius of gyration $R_{g,chain} = 10$ nm; the ratio of the excess scattering length of the sphere to that of one attached chain is $\rho_S/\rho_C = 10$ (thus, the excess scattering length of the sphere is only one-fifth of the total excess scattering length). The structure factor[38] $S(q)$ is for a radius of the excluded volume hard sphere interaction $R_{HS} =$ 35 nm and a volume fraction of such hard spheres $\phi_{HS} = 0.25$, not far from the hard sphere crystallization transition. The parameters are not least-squares optimized but have rather independent effects on the shape of the scattering function. We also find that a replacement of $S(q)$ by that of an adhesive hardsphere potential[38] likely cannot improve the fit. There remains obviously some ambiguiety which model is the right one, with a critical different outcome. The parameters of the micelle model seem to be reasonable. More extended measurements at lower q or microscopy results would be required to sort something out.

TABLE 3: Hierarchically Branched Chain Model (Eq 4) Fitting Parameters for SAXS Data of Coacervates (Fits in Figure 9a)

Φ	$R_{g,1}$/nm	$R_{g,2}$/nm[a]	ϕ_1^{-1} [a]	$[(4\pi/3)\phi_1^{-1}]^{1/3}$	$R_{g,IFT}$/nm
13.3	2.47 ± 0.04	≥40	≥340	≥11	18.9 ± 0.7
6.67	2.67 ± 0.01	≥45	≥ 80	≥ 7	16.3 ± 2.0
2.67	2.91 ± 0.06	≥38	≥280	≥10	17.9 ± 0.4
1.33	3.02 ± 0.22	≥44	≥610	≥13	18.3 ± 0.5

[a] Minimum values of highly linear dependent. ϕ_1^{-1}, $R_{g,2}$ which can fit the data.

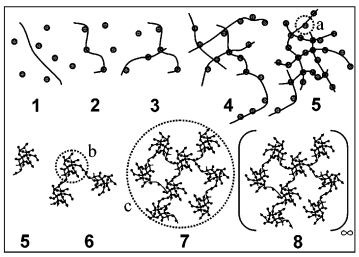

Figure 10. Proposed distribution of excess dendrimers (gray spheres) and linear polyelectrolyte (black lines), schematic. **1** independent dendrimer and polyelectrolyte; **2** transient IPEC (dendrimer can move along the chain); **3** IPEC with transient cross-link (dendrimer polycation); **4** first microgel (still high net negative charge); **5** almost neutral IPEC with partially collapsing center; critical size/charge ratio for attraction between microgels is reached; **6** "intermolecular" microgel cluster; **7** overcharged microgel cluster, evtl. charge stabilized; **8** coagulated microgels (coacervate). The dotted circles indicate three blob sizes: that of a dendrimer attached to the chain, that of a dense gel inhomogeneity, and that of the entire microgel cluster.

Model of IPEC Formation and Coacervate Formation. In Figure 10, we propose a possible model for the subsequent associative micro- and macrophase separation in the system. Independent dendrimer and strongly self-avoiding polyelectrolyte **1** interact attractively upon protonation of the dendrimer to form transient "monomolecular" IPECs **2**, and the entire IPEC remains highly negatively charged but with positively charged patches localized at the side of the dendrimer away from the chain. Thus, the dendrimer polycation can form a transient cross-link between two polyelectrolyte chains, which preferably spread from the cross-link in different directions—the first step to multimolecular IPECs **3**. Aggregation to microgels **4** will be limited by their net charge, accumulating a dense cloud of counterions which is osmotically unstable against a more even distribution of the charge in the system. The electroneutrality of the IPEC is more important in the interior of the microgel, whereas a charge imbalance in the less dense periphery can be compensated by a rather diffuse ionic cloud. When the net charge of the IPEC is almost zero (because of enhanced dendrimer protonation), the missing electrostatic repulsion among branches in the periphery and the high molecular weight of the IPECs **5** make them unstable against colloidal aggregation, at a critical size versus charge ratio. This ratio is reached at the onset of the second stage. When the microgels stick together to microgel clusters **6** and **7**, a complete collapse of the first fractal structure is possibly hindered by two reasons. First, the multiple cross-links (although each one is reversible) in any microgel domain are cooperatively coupled and thus practically irrevers-

ible, making the swelling and deswelling of the microgels time-consuming processes. Second, the residual IPEC charges (either still negative or already positive because of overcharging or both because of sterical hindrance for optimum ion pairing) need to be compensated by small counterions in their vicinity. Water-rich domains with a large total volume are thus still required for accommodation of these counterions. The microphase separation of the IPEC cluster is favored against a homogeneous structure with too many small water channels. The result is likely a hierarchically branched structure **7** with two mesh sizes, the smaller one given by the dendrimer number density required to form a neutral IPEC (core regions) when the interconnecting chains are in swelling equilibrium, and the larger one by the equilibrium distance between the cores, given by the balance between attractive potentials between microgels **5** and the repulsive interaction of their ionic clouds. The third length, the average diameter of the IPEC clusters, is probably only kinetically controlled (by a depletion mechanism). The equilibrium would be reached at a macroscopic phase separation to the coacervate **8** through coagulation of microgel clusters **7**, leaving an upper phase with only sporadically clustered microgels **5**.

5. Conclusions

We explored the structure of the colloids in an IPEC forming mixture of polyelectrolyte and dendrimer on the mesoscopic scale by light scattering and on the microscopic scale by SAXS. A model describing the structural evolution of the polyelectrolyte association and microphase separation during dendrimer charging is proposed and checked against the present scattering results. IPEC formation proceeds in two major stages. Monomolecular and multimolecular IPECs with a critical size versus charge ratio are subsequently formed upon charging of the dendrimer guest polyelectrolyte (GPE). In a second stage, the critical IPECs with a molecular weight of 10^6 g/mol undergo colloid aggregation and form microgels with diameters of 1−2 μm and molecular weight about 10^8 g/mol, dependent on the polymer concentration. The microgel inhomogeneities are highly swollen. At higher polyelectrolyte concentration, microgels are eliminated to form a separate coacervate phase. The microstructure of microgel and coacervate was similar, as concluded from yet ambiguous SAXS data fitting: a randomly branched gel with an R_g of the mesh between 2.4 and 3 nm, decreasing with increasing GPE excess, and an R_g of inhomogeneities larger than 20 nm, or a sticky copolymer micellelike structure. The ambiguity, mostly resulting from low-q upturns, will have to be resolved by more extended scattering or microscopy studies.

Acknowledgment. This work was financially supported by the Mitsubishi Foundation and by Grant-in-Aid for Scientific Research No. 11650928 from the Ministry of Education, Science, and Culture, Japan.

References and Notes

(1) Xia, J.; Dubin, P. L. In *Macromolecular Complexes in Chemistry and Biology*; Dubin, P., Bock, J., Davies, R. M., Schulz, D. N., Thies, C., Eds.; Springer: Berlin, 1994; Chapter 15, pp 247−71.
(2) Morawetz, H.; Hughes, W. L. *J. Phys. Chem.* **1952**, *56*, 64.
(3) Napper, D. *Polymeric Stabilization of Colloid Dispersions*; Academic Press: London, 1983.
(4) Likos, C. N.; Vaynberg, K. A.; Löwen, H.; Wagner, N. J. *Langmuir* **2000**, *16*, 4100.
(5) Pillai, O.; Panchagnula, R. *Curr. Opin. Chem. Biol.* **2001**, *5*, 447.
(6) Gebhart, C. L.; Kabanov, A. V. *J. Contr. Relat.* **2001**, *73*, 401.
(7) Hammond, P. T. *Curr. Opin. Colloid Interface Sci.* **2000**, *4*, 430.
(8) Picart, C.; Lavalle, Ph.; Hubert, P.; Cuisinier, J. G.; Decher, G.; Schaaf, P.; Voegel, J.-C. *Langmuir* **2001**, *17*, 7414.
(9) Ferreira, M.; Rubner, M. F. *Macromolecules* **1995**, *28*, 7107.
(10) Sullivan, D. M.; Bruening, M. L. *J. Am. Chem. Soc.* **2001**, *123*, 11805.
(11) Dubas, S. T.; Farhat, T. R.; Schlenoff, J. B. *J. Am. Chem. Soc.* **2001**, *123*, 5368.
(12) Krasemann, L.; Toutianoush, A.; Tieke, B. *J. Membr. Sci.* **2001**, *181*, 221.
(13) Mizusaki, M.; Morishima, Y.; Dubin, P. L. *J. Phys. Chem. B* **1998**, *102*, 1908.
(14) Wang, Y.; Kimura, K.; Dubin, P. L.; Jaeger, W. *Macromolecules* **2000**, *33*, 3324.
(15) Mizusaki, M.; Morishima, Y.; Yoshida, K.; Dubin, P. L. *Langmuir* **1997**, *13*, 6941.
(16) Wang, Y.; Kimura, K.; Dubin, P. L.; Jaeger, W. *Macromolecules* **2000**, *33*, 3324.
(17) Zhang, H.; Dubin, P. L.; Ray, J.; Manning, G. S.; Moorefield, C. N.; Newkome, G. R. *J. Phys. Chem. B* **1999**, *103*, 2347.
(18) Brown, M. D.; Schätzlein, A. G.; Uchegbu, I. F. *Int. J. Pharm.* **2001**, *229*, 1.
(19) Gebhart, C. L.; Kabanov, A. V. *J. Contr. Relat.* **2001**, *73*, 401.
(20) Kabanov, V. A. In *Macromolecular Complexes in Chemistry and Biology*; Dubin, P., Bock, J., Davies, R. M., Schulz, D. N., Thies, C., Eds.; Springer: Berlin, 1994; Chapter 10, pp 151−174.
(21) Prosa, T. J.; Bauer, B. J.; Amis, E. J. *Macromolecules* **2001**, *34*, 4897.
(22) Nisato, G.; Ivkov, R.; Amis, E. J. *Macromolecules* **2000**, *33*, 4172.
(23) Welch, P.; Muthukumar, M. *Macromolecules* **2000**, *33*, 6159.
(24) Chen, W.; Tomalia, D. A.; Thomas, J. L. *Macromolecules* **2000**, *33*, 9169.
(25) Pezron, E.; Leibler, L.; Lafuma, F. *Macromolecules* **1989**, *22*, 2656.
(26) Xia, J.; Zhang, H.; Rigsbee, D. R.; Dubin, P.; Shaikh, T. *Macromolecules* **1993**, *26*, 2759.
(27) Kabanov, V. A.; Zezin, A. B.; Rogacheva, V. B.; Gulyaeva, Zh. G.; Zansochova, M. F.; Joosten, J. G. H.; Brackman, J. *Macromolecules* **1999**, *32*, 1904.
(28) Menger, F. M.; Sykes, B. M. *Langmuir* **1998**, *14*, 4131; see also references therein.
(29) Menger, F. M.; Peresypkin, A. V.; Caran, K. L.; Apkarian, R. P. *Langmuir* **2000**, *16*, 9113.
(30) Menger, F. M.; Seredyuk, V. A.; Apkarian, R. P.; Wright, E. R. *J. Am. Chem. Soc.* **2002**, *124*, 12408.
(31) Stuart, M. A. C.; Besseling, N. A. M.; Fokkink, R. G. *Langmuir* **1998**, *14*, 6846.
(32) Feigin, L. A.; Svergun, D. I. In *Structure Analysis by Small-Angle X-ray and Neutron Scattering*; Taylor, G. W., Ed.; Plenum Press: New York, 1987.
(33) Glatter, O. *J. Appl. Crystallogr.* **1977**, *10*, 415.
(34) Svergun D. I. *J. Appl. Crystallogr.* **1991**, *24*, 485.
(35) Svergun D. I. *J. Appl. Crystallogr.* **1992**, *25*, 495.
(36) Burchard, W. *Macromolecules* **1977**, *10*, 919.
(37) Pedersen, J. S.; Gerstenberg, M. C. *Macromolecules* **1996**, *29*, 1363.
(38) Pedersen, J. S. *Adv. Colloid Interface Sci.* **1997**, *70*, 171.
(39) Hecht, A.-M.; Horkay, F.; Geissler, E. *J. Phys. Chem. B* **2001**, *105*, 5637.
(40) Zintchenko, A.; Dautzenberg, H.; Tauer, K.; Khrenov, V. *Langmuir* **2002**, *18*, 1386.
(41) Nishio, T. *Biophys. Chem.* **1998**, *71*, 173.
(42) Nagasawa, M.; Holtzer, A. *J. Am. Chem. Soc.* **1964**, *86*, 538.
(43) Calculated from values in *CRC Handbook of Chemistry and Physics*, 64th ed.; 1984; p D-257.
(44) Simmons, C.; Webber, S. E.; Zhulina, E. B. *Macromolecules* **2001**, *34*, 5053.
(45) Glatter, O. In *Neutron, X-Ray and Light Scattering*; Lindner, P., Zemb, Th., Eds.; North-Holland: Amsterdam, 1991; pp 33−82.
(46) Stechemesser, S.; Eimer, W. *Macromolecules* **1997**, *30*, 2204.
(47) Blanco, M. C.; Leisner, D.; Vázquez, C.; López-Quintela, M. A. *Langmuir* **2000**, *16*, 8585.
(48) Brochard, F.; de Gennes, P. *Macromolecules* **1977**, *10*, 1157.
(49) Furukawa, H. *Physica A* **1984**, *123*, 497.